Coordination-dependent tight-binding potentials for carbon-based materials

1995 J. Phys.: Condens. Matter 7 4019

(http://iopscience.iop.org/0953-8984/7/21/003)

J. Phys.: Condens. Matter 7 (1995) 4019–4031. Printed in the UK

Coordination-dependent tight-binding potentials for carbon-based materials

S Serra, C Molteni† and L Miglio
Dipartimento di Fisica dell'Università di Milano, via Celoria 16, I-20133 Milano, Italy.

Received 16 January 1995

Abstract. We point out the important role of coordination-dependent terms in tight-binding potentials for carbon structures, as required by the strong changes in orbital hybridization, especially for low-coordination phases. We discuss the performances of two forms of potential on the basis of the cohesion energy and molecular dynamics predictions, as compared with existing first-principles results.

1. Introduction

It is well known that carbon displays rather stable structures with different coordination numbers: 4 (diamond), 3 (graphite), 2 (carbon chains). This flexibility is achieved by hybridizing the atomic orbitals in sp^3, sp^2, sp configurations, so that three-dimensional, planar and linear structures, respectively, are obtained. The recent discovery of fullerenes [1] has confirmed the high allotropic inclination of carbon, as their bonding configuration is in between sp^3, and sp^2 hybrids. In the common pair potential scheme, the total energy of the system is rather sensitive to the number of neighbours, the repulsive energy being proportional to the coordination number. This is not the case for graphite and diamond, for example; therefore it is quite clear that coordination dependence of the interatomic potentials is an important issue for carbon.

This problem has been pointed out by Tersoff (formerly for silicon and subsequently for carbon) [2] in the framework of a classical potential composed for a simple repulsive part and a complex attractive one. In that approach, however, the latter term bears most of the coordination-dependence, where the angles between bonds have also been considered in quite a cumbersome expression.

The advantage of tight-binding (TB) potentials is that three-body effects are naturally included in the attractive part, via a Slater–Koster [3] expansion of the TB hopping elements into angular and radial contributions. Two recent studies by Goodwin [4] and Xu *et al* [5] have demonstrated that TB potentials for carbon work fairly well, provided that the radial dependence of the hopping elements and the two-body repulsive potential are smoothly set to zero at large interatomic distances. Nonetheless, crystalline phases other than diamond and graphite do not display a satisfactory agreement with first-principles calculations of the cohesion energy curves [6]. For high-coordination (unstable) phases, this is probably due to an overestimation of the repulsive contribution, which scales linearly with the coordination number. However, for the linear chain, we think that the limitations come from the TB part,

† Present address: Cavendish Laboratory, Madingley Road, Cambridge CB3 OHE, UK.

0953-8984/95/214019+13$19.50

which bears an intrinsic reference to the diamond structure. The hopping terms, in fact, are fitted to the equilibrium bands of diamond and, even if a suitable scaling law is adopted for their radial dependence, it is difficult to reproduce the strong dehybridization occurring in the sp configuration.

This deficiency is not easily dealt with by adding more pairwise terms into the repulsive potential (as it is in the work of Xu *et al* [5]), nor by constructing a complicated coordination dependence into it (as was done by Mercer and Chou [7] for example, in the case of silicon and germanium).

It is our opinion that the physical intelligibility of TB potentials is preserved only if a limited set of parameters is used and, in turn, making such a choice is possible only if the important physical effects are correctly included in the potential. In this paper we present two TB potentials which include correction terms for coordination changes with respect to the diamond phase, both as an effective rescaling of the total potential depth and as a separate adjustment of the attractive and the repulsive parts.

A good reproduction of the cohesion energy curves for all the low-coordination phases is obtained in the first, simpler case. The second form yields a very satisfactory agreement with the first-principles curves [6] from the linear chain up to the FCC coordination, still with a limited set of parameters.

In the next two sections we outline our potentials and comment on their physical meaning. Finally, in the last section, total energy predictions for small clusters and molecular dynamics simulations of liquid carbon are reported; they compare quite well with previous first-principles results.

2. A first step towards coordination-dependent potentials

Within a TB approach, the total energy is partitioned as

$$E_{\mathrm{tot}} = 2\sum_{\nu,k}^{\mathrm{occ}} \varepsilon_\nu(k) + \frac{1}{2}\sum_{i,j} U(r_{ij}) \tag{1}$$

where the $\varepsilon_\nu(k)$ are the eigenvalues of the TB matrix. They generate the attractive, covalent contribution to the cohesive energy (hereafter this will be indicated as the band-structure energy, E_{bs}). The factor 2 in the first term takes into account the spin degeneracy, whereas ν and k label the bands and the wavevectors, respectively. The repulsive contribution stemming from the overlap between occupied orbitals is represented by the second term in (1) (hereafter indicated as E_{rep}), where $U(r_{ij})$ is a short-range, central interaction between atom i and atom j:

$$U(r_{ij}) = \phi g(r_{ij}) \tag{2}$$

and

$$g(r_{ij}) = \left(\frac{r_0}{r_{ij}}\right)^p$$

with r_0 indicating the equilibrium distance between nearest neighbours and $p \in \Re$.

The set $\varepsilon_\nu(k)$ implicitly depends on the atomic positions through the Slater–Koster parametrization of the hopping elements in the TB matrix. The latter are given in terms of two-centre integrals $V_{\mathrm{ss}\sigma}$, $V_{\mathrm{sp}\sigma}$, $V_{\mathrm{pp}\sigma}$, $V_{\mathrm{pp}\pi}$ for sp-bonded materials and cosine directors between pairs of atoms. The radial dependence of V_{llm} (l = s, p and $m = \sigma, \pi$) is given

by scaling the equilibrium values V^0_{llm} with a suitable function of the interatomic distance $f(r_{ij})$:

$$V_{llm} = V^0_{llm} f(r) \tag{3}$$

and

$$f(r) = \left(\frac{r_0}{r}\right)^q$$

where $q = 2$ in the usual Harrison scheme [9]. In this case, we used the Chadi parameters V^0_{llm}, as reported in [8], and scaled them according to the Harrison scheme. In the following we will refer to q and p as the exponents of the scaling laws of the attractive and repulsive parts of the potential, respectively.

In spite of the fact that our total energy in (1) fits the cohesive energy curve of one single phase (diamond, for example) very well, it is not possible to get a good reproduction of the whole set of curves for different phases, especially at very low and very high coordination. This problem does not originate merely from the limitation of the set of parameters, since the functional form of the potential itself is not adequate for reproducing the relevant changes of the parameters with the coordination number.

In a very interesting note that appeared in 1983 [11], Robertson pointed out that the Harrison prescription for the scaling law of the hopping elements is not suitable for use in the estimation of the actual changes in $V_{pp\pi}$ from sp^3 diamond to sp^2 graphite, as indicated by the corresponding band dispersion relations. This is clearly related to the fact that dehybridized p_z orbitals play different roles in the planar structure and in the tetrahedral configuration. As a consequence, the scaling of E_{bs} is not appropriate even from diamond to graphite and a correction term is needed. A related modification is recommended also for E_{rep}, since it originates from the orbital overlap and is very probably affected by the orbital hybridization.

A first attempt to include both corrections into one single term to add to (2) can be made by selecting a weak dependence on the interatomic distance, so that the main effect will turn out to be an energy rescaling with coordination z. Accordingly, E_{tot} is then rewritten as

$$E_{tot} = 2\sum_{\nu,k}^{occ} \varepsilon_\nu(k) + \frac{1}{2}\sum_{ij} U(r_{ij}) + \frac{1}{2}\sum_{ij} U'(z, r_{ij}) \tag{4}$$

with

$$U'(z, r_{ij}) = \varphi b(z)\left(\frac{r_0}{r_{ij}}\right) \tag{5}$$

and

$$b(z) = (1 + \beta z^n)^{-1/2n}. \tag{6}$$

The coordination-dependent prefactor $b(z)$ is very similar to the Tersoff expression [2], even if the parameters β and n are numerically different. They are fitted, along with ϕ, φ and p, onto the equilibrium values of the first-neighbour distance in diamond (r_0^{dia}) and in the graphite (r_0^{gra}), the bulk modulus (B^{dia}) and the cohesion energy differences among the relevant phases ($\Delta E^{cohes.}_{dia-gra}$, $\Delta E^{cohes.}_{dia-lc}$). We have obtained $\phi = 13.079$ eV, $\varphi = 7.014$ eV, $p = 3.432$, $\beta = 0.1$ and $n = 2.785$.

By retaining only the first neighbours in equation (4), we note that this correction term is proportional to $z^{1/2}$ for large values of z, whereas a nearly linear dependence is produced at low coordinations. This feature is consistent with the fact that hybridization changes are more important in the latter case.

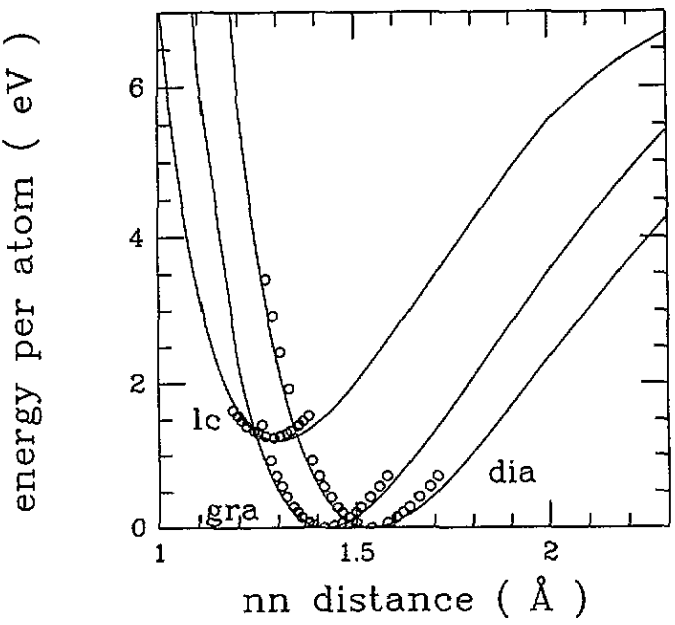

Figure 1. Cohesive energies of diamond, graphite and linear chains as referred to the equilibrium cohesive energy of the diamond phase. Solid lines show the calculation with potential A (see the text), and open circles show the *ab initio* results of [6].

In figure 1 the cohesive energies diagram obtained using our potential are compared with first-principles results obtained by Fahy and Louie [6]. We note that a fairly good agreement is obtained at low coordinations (position and curvature), but the results for BCC and FCC structures are no better than those obtained using the 24-parameter potential of Xu *et al* [5]. Still, our potential requires a much lower number of parameters than of [5] and satisfactory predictions via total energy or molecular dynamics simulations are possible, especially for average coordinations <6, as is the case for the liquid carbon results reported in Section 3. In the following sections we will refer to it as potential A.

3. A flexible potential for carbon structures

In order to overcome some of the shortcomings outlined above, we derived a different form of potential with the following features.

(i) For the diamond phase it reduces to the usual expression (1) with (2) and (3), where suitable values of ϕ, q and p are chosen in order to get the best agreement with the cohesion energy curve, as calculated from first principles.

(ii) Coordination-dependent corrections are operated both in the attractive and in the repulsive terms, since they scale with interatomic distance according to different power laws (p and q are rather different).

(iii) A smooth drop of the TB interactions and the repulsive potentials is introduced for large interatomic distances, since inverse-power-law decay is not suitable for molecular dynamics simulations, where the forces need to be zero at a certain cut-off radius.

We started by accurately fitting $\phi_1 \equiv \phi_1^{\rm dia}$, q, p onto $r_0^{\rm dia}$, $B^{\rm dia}$ and $E_{\rm coh}^{\rm dia}$, the cohesive

energy of the diamond phase, as provided by [6]. In our scheme, E_{bs} is actually rescaled as

$$\sum_{\nu,k} \varepsilon_\nu(k) - \sum_i \varepsilon_{ii}^0 n_i^0 \tag{7}$$

where the ε_{ii}^0 are the on-site energies in the bulk configuration that we take to be constant in our simulations and n_i^0 are the occupation numbers in the atomic configuration. Obviously, the second term in (7) does not correspond to the real atomic limit—its role is just intended to be that of fixing a reasonable energy reference for our potential—so it is zero at very large distances and small at the cut-off radius.

The TB parameters for V_{ilm}^0 are here taken to be the ones given by Papaconstantopoulos [12], since they provide a ratio p/q which is closer to 2 than the Chadi parameters; this choice is indicated as being appropriate by the orbital overlap origin of the repulsive potential [10]. In fact, we obtain $q = 2.61$, which is actually larger than the Harrison prescription ($q \sim 2$) for sp-bonded materials, and the repulsive exponent p turns out to be 4.098. The former is in very good agreement with accurate calculations of the scaling law for silicon performed by Mercer and Chou [7], on the basis of the first-principles band changes for hydrostatic deformation of the diamond structure. This guarantees that E_{bs} is well reproduced for diamond. The good agreement with the overall curvature of the cohesive energy curve obtained by first-principles methods confirms the quality of our fit for the repulsive part.

Coordination-dependent terms should be included now in the TB matrix, in order to take into account the objections of Robertson. However, it is much easier to add a term like

$$\Delta E_{bs} = \phi_2(z)\left(\frac{r_0}{r}\right)^q \tag{8}$$

to the band-structure energy, which displays such features: it scales with r like $E_{bs}(r)$ (same q), and $\phi_2(z)$ is defined to be zero for $z = 4$. It is possible to obtained its behaviour for $z \neq 4$ via a fitting to the cohesion energy diagram for different coordinations (see figure 2), as will be described later. Anyway, it is very likely that $\phi_2(z)$ will be positive both for low and for high coordinations since sp^3 and sp^2 configurations are actually the most cohesive ones (largest overlap).

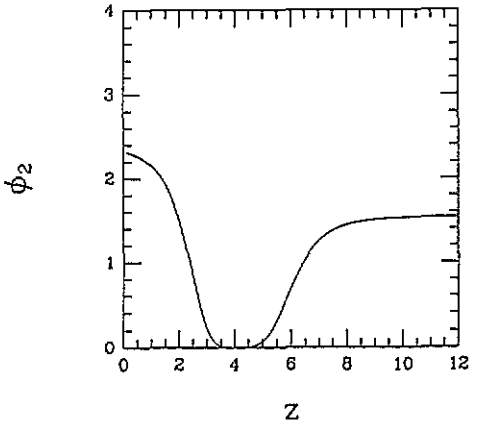

Figure 2. ϕ_2 as a function of the coordination number z.

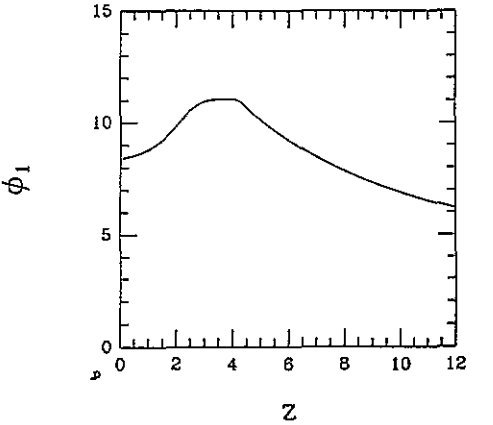

Figure 3. ϕ_1 as a function of the coordination number z.

For the repulsive term, it is better to let the prefactor ϕ_1 depend on the coordination (see figure 3) in such a way that

$$\phi_1(z=4) = \phi_1^{dia}. \tag{9}$$

This is a reasonable choice—also used by Sawada for the silicon case [13]—since it does not add new terms into the potential and the same scaling law with respect to interatomic distance as for the diamond phase is also preserved.

Actually, our choice to scale the correction terms for the attractive and the repulsive part with the same functional dependence as the diamond phase is not an oversimplification, since small deformations around any equilibrium structures are very well described by the Harrison-like inverse-power law. At larger interatomic distance, outside the usual equilibrium situations, a smooth cut-off function is, however, necessary.

We have used the Goodwin–Skinner–Pettifor cut-off function [14],

$$t_\gamma(r) = \exp\left(\gamma\left[-\left(\frac{r_0}{r}\right)^{n_c} + \left(\frac{r_0}{r_c}\right)^{n_c}\right]\right) \tag{10}$$

with $\gamma = p, q$ for the repulsive and attractive parts of the potential, respectively. We optimized the values of r_c and n_c to get the best reproduction of the total energy curvature for high-coordination phases (large interatomic distances), obtaining $n_c = 9$ and $r_c = 2.65$.

The final expression of our TB potential is therefore

$$E_{tot} = \sum_{\nu,k} \varepsilon_\nu(k) + \frac{1}{2}\sum_{i,j}{}' \phi_2(z)\left(\frac{r_0}{r_{ij}}\right)^q t_q(r_{ij}) + \frac{1}{2}\sum_{i,j}{}' \phi_1(z)\left(\frac{r_0}{r_{ij}}\right)^p t_p(r_{ij}) \tag{11}$$

where $\sum'$ indicates the sum over first-nearest neighbours only. We are now left with the problem of fitting the proper functional dependence of ϕ_1 and ϕ_2 on coordination. This can be achieved by selecting suitable values of ϕ_1 and ϕ_2 for each phase between $z = 2$ and $z = 12$, so that expression (11) matches the corresponding equilibrium lattice parameters and cohesion energies for the diamond phase. We obtain two numerical sets for $\phi_1(z)$ and $\phi_2(z)$ which can be interpolated using the following tool functions:

$$\phi_2(z) = \frac{\delta(|z-4|)^\gamma}{1+\beta(|z-4|)^\gamma} \tag{12}$$

$$\phi_1(z) = \phi_1^{\mathrm{dia}} - \frac{\delta'(|z-4|)^{\gamma'}}{1+\beta'(|z-4|)^{\gamma'}}. \tag{13}$$

In figure 2 and 3 we display $\phi_2(z)$ and $\phi_1(z)$, respectively. We note that ΔE_{bs} varies significantly for $1 < z < 3$ and $5 < z < 7$, where a sizeable change in hybridization is expected with respect to the most stable situations (sp^3 and sp^2 configurations). For $z > 7$ it is reasonable to find no significant change in ϕ_2.

For $\phi_1(z)$—see figure 3—we have nearly specular behaviour, with the maximum value for $z = 4$. This is consistent with the fact that the most cohesive configuration ($z = 4$) is determined by the largest overlap between hybridized, neighbouring orbitals and this, in turn, generates the largest repulsion as due to their occupation. Also at variance with figure 2, there is a smooth decrease in figure 3 for $z > 6$, which shows that the straightforward pair counting of the two-body repulsion (actually a many-body term) overestimates E_{rep} at high coordinations. It is interesting to note that this difference between $\phi_1(z)$ and $\phi_2(z)$ generates a behaviour with z of $\Delta E_{bs} + E_{rep}$ which is roughly linear in the case of low coordination and is weaker in the case of high coordination, as for potential A. In tables 1 and 2 we report the actual values of the parameters occurring in expressions (13), and (12), respectively.

Table 1. Values of parameters of the ϕ_2-function.

ϕ_2	$z < 4$	$z > 4$
δ	0.242	0.0723
β	0.101	0.
γ	4	4.108

Table 2. Values of parameters of the ϕ_1-function.

ϕ_1	$z < 4$	$z > 4$
δ'	0.1261	1.072
β'	0.0436	0.126
γ'	4	1.133

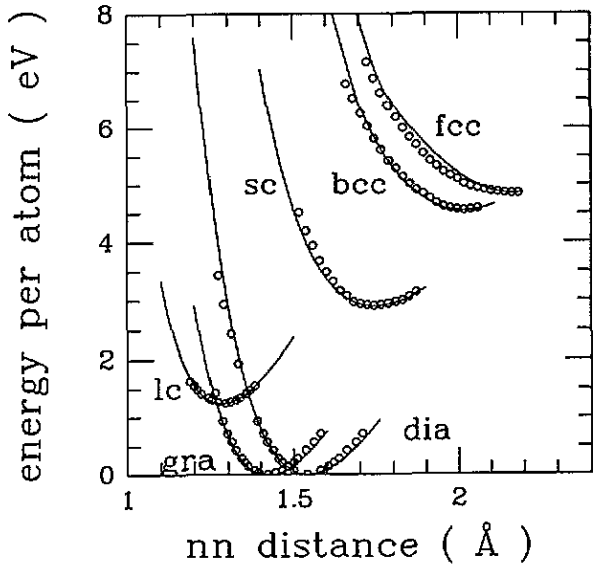

Figure 4. Cohesive energies of diamond, graphite, linear chains, SC, BCC and FCC structures ,as referred to the equilibrium cohesive energy of the diamond phase. Solid lines show the present calculation with potential B (see the text) and open circles show the *ab initio* results of [6].

In figure 4 we show the total energy curves from the linear chain up to the FCC phase. It is clear that there is a very good agreement with the *ab initio* results for all phases, and also the curvatures around the minima are nicely reproduced without any fitting. In the following sections we will refer to this potential as B.

One final comment should be added $\phi_2(z)(r_0/r)^q$ is a correction to E_{bs} which does not depend on the bond angles, unlike a genuine TB contribution. In fact this is not a problem for high coordinations; nonetheless for $z \leqslant 2$ (outside the range of our interpolation) a sizeable contribution from dehybridized π-orbitals is likely to appear when the π-bonds are bent into a ring formation from finite chains. In the next section we will generalize the notion of coordination and we will show how to include angular terms properly in the term $\phi_2(z)$.

4. Local effective coordination and the π-orbital's bending energy

So far we have used the two potentials (A and B) in total energy calculations for infinite crystalline phases, where the coordination number is a well defined constant for each structure. In molecular dynamics (MD) simulations the coordination of any atom can change continuously with time. Besides this, the presence of rather different coordinations on a local scale, as in small clusters for example, indicates the need for a more refined definition of the coordination number. In order to overcome these problems we introduce the local effective coordination of the ith atom $z(i)$ as the weighted number of atoms inside a suitable sphere of radius $r_0 + d_0$ (here $r_0 \sim 2.1$–2.2 Å, d_0 can be selected freely from the range $0 < d_0 < 0.1$ Å):

$$z(i) = \sum_{ij} f_c(r_{ij}) \tag{14}$$

with

$$f_c(r) = \begin{cases} 1 & \text{if } r < r_0 - d_0 \\ \frac{1}{2}[1 - \sin(\pi(r - r_0)/2d_0)] & \text{if } r_0 - d_0 < r < r_0 + d_0 \\ 0 & \text{if } r > r_0 + d_0. \end{cases} \tag{15}$$

In order to preserve the action–reaction principle for each pair of atoms (i, j) we have used the mean value of the effective coordination:

$$z(i, j) = \frac{1}{2}(z(i) + z(j)). \tag{16}$$

With this definition any kind of system with arbitrary coordination can be simulated. In particular, for the crystalline phases the effective coordination coincides with the actual coordination number.

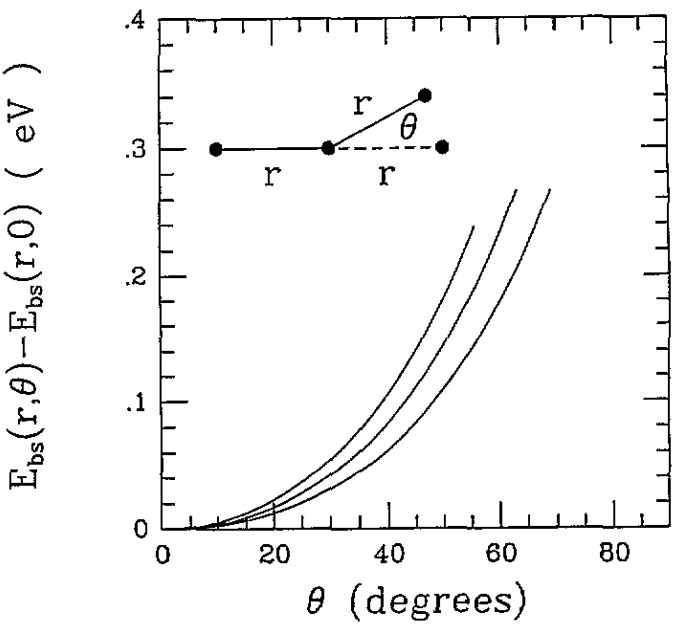

Figure 5. E_{bs} for a trimer as a function of the angle θ between neighbouring bonds at fixed interatomic distance.

In the case of potential B we have already pointed out that angular dependence in $\phi_2(z)$ can be important for rings. In order to take it properly into account, we have determined the angular dependence of E_{bs} for a chain as a function of the angle between two bonds. In figure 5 we show the results for E_{bs} for a trimer where we have varied the angle θ with respect to the chain axis at a fixed interatomic distance r_{ij}. Similar results are found for different values of interatomic distances, so a simple law for the angular dependence of the band structure can be inferred:

$$E_{bs}(r,\theta) = E_0(r) + \alpha(r)(1 - \cos^2(\theta)) \tag{17}$$

with $\alpha(r) > 0$. This holds in the particular case of the trimer, with the polar coordinate system suitably chosen; in any case, it can be easily generalized for generic cartesian axes. In this case we must introduce the general expression

$$\cos(\theta) = -(l_1 l_2 + k_1 k_2 + m_1 m_2) \tag{18}$$

where $l_{1,2}$, $k_{1,2}$ and $m_{1,2}$ are the cosine directors of the two bonds around the pivot atom in the chain. It is important to note that expression (18) has the same form as appears in the Slater–Koster expansion of the hopping terms for π-orbitals. Therefore we are confident that the physical effect of π-orbital bending is properly included if ΔE_{bs} is now rewritten as

$$\Delta E_{bs} = \phi_2(z_{ij})\left[1 + \eta(1 - A_{ij}) f_d(z_{ij})\right]\left(\frac{r_0}{r_{ij}}\right)^q t_q(r_{ij}) \tag{19}$$

where $\phi_2(z_{ij})$ is the same as before, η is a constant equal to 1.4 and f_d is given by

$$f_d(z) = 1/[\exp((z - z_0)/dz) + 1] \tag{20}$$

with $z_0 = 1.89$, $dz = 0.1$, so that the angular contribution is quenched for coordinations higher than 2. The term A_{ij} contains the angular dependence and is constructed as an average of $\cos^2\theta$ and $\cos^2\theta'$, where θ and θ' are the angles between the two bonds around atom i (ii' and ij) and j (jj' and ji), respectively:

$$A_{ij} = \frac{1}{2}\left(\sum_{i'\neq j}(l_{ii'}l_{ij} + n_{ii'}n_{ij} + m_{ii'}m_{ij})^2 + \sum_{j'\neq i}(l_{jj'}l_{ji} + n_{jj'}n_{ji} + m_{jj'}m_{ji})^2\right). \tag{21}$$

It can be easily seen that in the case of trimers it gives the same functional expression as previously found for E_{bs}. In the next section we will test the reliability of our scheme for prototypical systems with mixed coordinations: small clusters and low-density amorphous and liquid carbon.

5. Molecular dynamics results

In the following we will give the results of MD simulations both on small clusters (C_2, ..., C_{10}) and on liquid and amorphous carbon. The inclusion of an effective local coordination is likely to play a key role in properly describing the features of low-density liquid and amorphous carbon, where coexistence of twofold-, threefold- and fourfold-coordinated atoms is found [15, 16, 17, 5].

The first set of results reported here are the ground-state properties of small carbon clusters. We have obtained good agreement with *ab initio* findings [19], as regards the trend of variation of the relative stability (figure 6) and of the bond lengths (table 3) with the number of atoms. In particular, we have found that both potentials, A and B, indicate a ring configuration to have higher stability than open segments with an even number

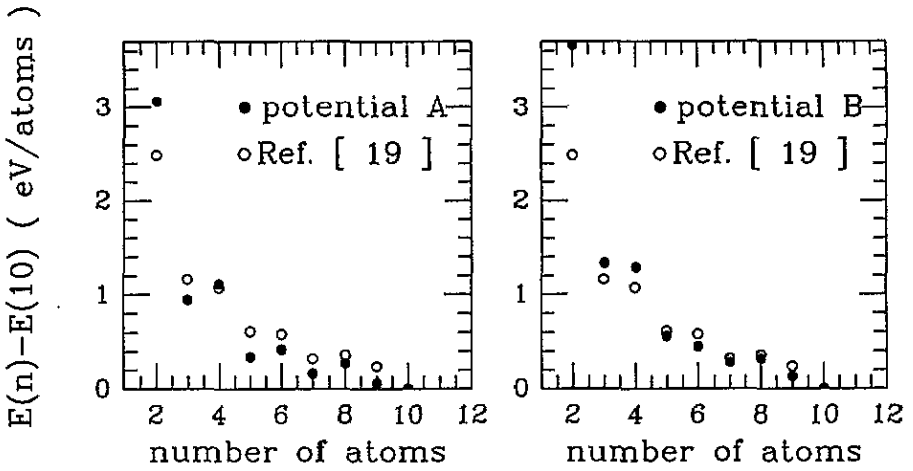

Figure 6. Cohesive energies of small clusters from C_2 to C_{10} (black dots), referred to the ground-state energy of C_{10}, by using potential A (left-hand panel) and potential B (right-hand panel). Open circles show the *ab initio* results of [19].

Table 3. Bond lengths of small clusters (C_2–C_{10}) as found using potential A (first row), potential B (second row) and *ab initio* results from [19].

	C_2	C_3	C_4	C_5	C_6	C_7	C_8	C_9	C_{10}
Potential A (Å)	1.15	1.29	1.295	1.25 1.33	1.31	1.23 1.29 1.35	1.22 1.44	1.23 1.27 1.31 1.36	1.3
Potential B (Å)	1.12	1.285	1.29	1.24 1.30	1.29	1.23 1.26 1.33	1.20 1.43	1.21 1.24 1.28 1.34	1.28
From [19] (Å)	1.24	1.28	1.42	1.271 1.275	1.33	1.27 1.26 1.28	1.24 1.38	1.269 1.261 1.269 1.283	1.29

of atoms larger than four. In fact potential B displays a qualitative agreement with the Hartree–Fock results [19] which justifies the additional contribution of π-orbital bending, but for the dimer—which represents an extremal condition. These results were obtained by means of a standard simulated annealing technique, which consists in an extremely slow quenching from high initial temperature of about ~2000–3000 K, down to 0 K. By taking full advantage of the low computational cost of the present MD scheme, we were able to perform long simulations (10^5 time steps) and with a relatively large time step (5×10^{-16} s).

In the second set of figures (figure 7–9), we show the structural and the electronic properties of liquid and amorphous carbon at low density (2 g cm^{-3}). These results were obtained by the following simulation strategies. First a well equilibrated liquid carbon sample was obtained by heating diamond in a cubic, periodically repeated simulation cell with 64 atoms, from 300 K up to 5000 K in 5000 time steps with a time step of 5×10^{-16} s. A careful equilibration of the sample was subsequently carried on at this temperature for

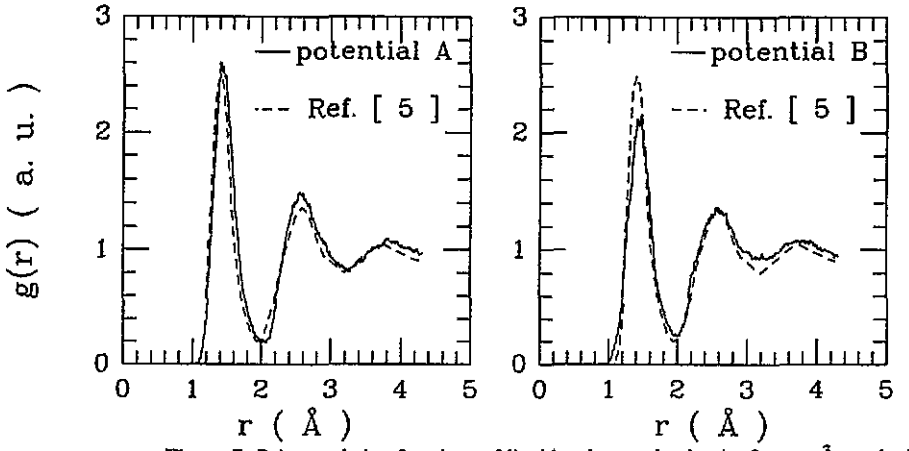

Figure 7. Pair correlation functions of liquid carbon at the density 2 g cm^{-3}, as obtained using potential A (solid line in the left-hand panel) and potential B (solid line in the right-hand panel). Here the one generated from another TB potential [5] is reported for comparison (dashed line).

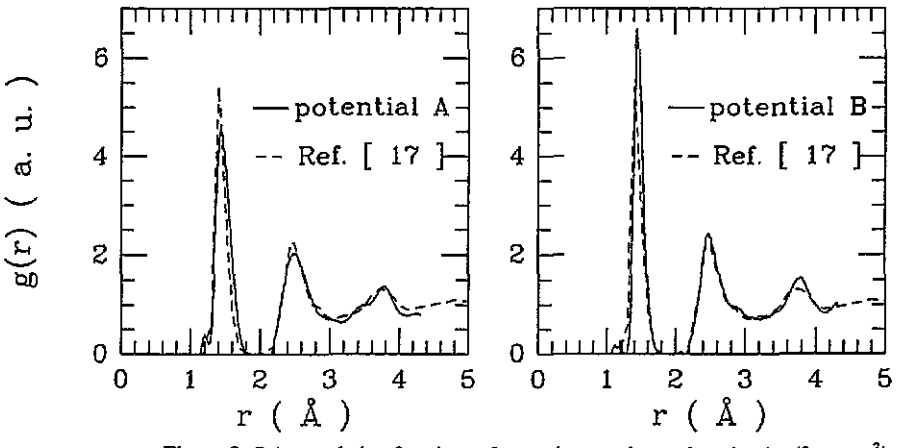

Figure 8. Pair correlation functions of amorphous carbon at low density (2 g cm^{-3}) as obtained using potential A (solid line in the left-hand panel) and potential B (solid line in the right-hand panel), compared to the one generated from another TB potential [17] (dashed line).

10^4 time steps. Finally we collected our data during a constant MD run as long as 3000 time steps. The results for the pair correlation function of the liquid with both potentials are shown in figure 7.

Amorphous carbon was subsequently obtained by quenching the liquid sample. In particular, we used the same quenching rate as in [17], i.e., we cooled the liquid carbon from 5000 K down to 700 K in 8000 time steps with a time step of 1×10^{-15} s. Then we collected our data for 3000 time steps at a constant temperature of 700 K. The resulting pair correlation functions and electronic densities of states are shown in figure 8 and figure 9, respectively. They show a rather good agreement with previous findings, [5, 17]. This is confirmed also by the analysis of other structural properties, like the bond-angle distribution function and coordination number, demonstrating a good transferability of our potentials. In fact, potential B gives pair correlation functions and coordination number distributions in better agreement with *ab initio* and experimental findings than potential A. In particular,

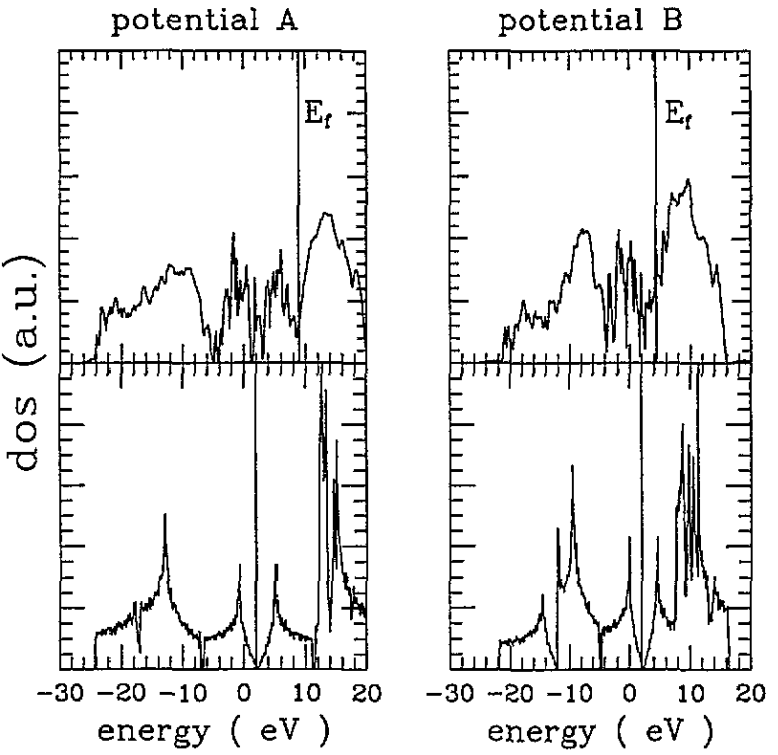

Figure 9. Electronic densities of states for amorphous carbon at low density (2 g cm^{-3}), for potential A (top left-hand panel) and potential B (top right-hand panel). The corresponding densities of states for graphite are displayed in the bottom panels.

we get a lower intensity for the peak in the pair correlation function corresponding to first neighbours, as in [15], and a smaller number of doubly coordinated sites than of fourfold coordinated ones (1% and 8% respectively) in the amorphous phase, in fine agreement with the experimental data of [18]. Obviously the great majority of the atoms in both of the amorphous samples are threefold coordinated, as is clear in figure 9 where we compare the electronic density of states of our amorphous samples (top) to the ones of graphite (bottom). We see that both potentials generate the appearance of bonding and antibonding π-states in the energy region where diamond displays the gap. The shape provided by potential B (top right-hand panel) is very similar to that from another TB calculation [17]: it shows only the broad peak of the bonding π-states below the Fermi level, since that for antibonding π-states is hidden by the broadening of the antibonding σ-states, as due to the disorder in the structure. Therefore we think that the TB parametrization adopted for potential B is superior to the one adopted for potential A. All our results demonstrate that an accurate description of all the cohesion energy curves appearing in the phase diagram is important in order to obtain superior quality MD results, even within a restricted coordination range.

6. Conclusions

The usual procedure for the generation of one interatomic potential is based on fitting a rather general parametric form onto a set of structural, elastic, vibrational data that is as large as possible. Recent TB potentials for carbon have been obtained along these lines.

However, as the number of parameters increases, the fitting algorithm spans a parametric hypersurface which becomes more and more complex. Most of the time the final result is far from being unique and little help is provided by the physical interpretation, since the precise role of each parameter cannot be assessed.

In this paper we presented an alternative path which is based on the assumption that the diamond phase is somehow a natural reference which can be represented by a rather simple potential form. Additional terms are introduced on a physical basis and the total number of parameters for the most general form is fairly limited. Preliminarily results of molecular dynamics simulations confirm the soundness of our scheme and provide a basis for more appealing simulations, outside the present range of first-principles methods.

Acknowledgments

We acknowledge partial financial support from the Italian National Research Council (CNR) under project No 94.00852.ct02 'Crescita, Caratterizzazione e Proprietà di Strutture Fullereniche', and the FORUM-INFM Institute for Condensed Matter Theory for computational support. One of us (SS) acknowledges the Scuola Normale Superiore (Pisa, Italy) for kind hospitality. We finally thank L Colombo (University of Milano) for helpful discussions on the molecular dynamics simulations.

References

[1] Kroto H W, Heath J R, O'Brien S C, Curl R F and Smalley R E 1985 *Nature* **318** 162
[2] Tersoff J 1988 *Phys. Rev. Lett.* **61** 2879
[3] Slater J C and Koster G F 1954 *Phys. Rev.* **94** 1498
[4] Goodwin L 1991 *J. Phys.: Condens. Matter* **3** 3869
[5] Xu C H, Wang C Z, Chan C T and Ho K M 1992 *J. Phys.: Condens. Matter* 4 6047
[6] Fahy S and Louie S G 1987 *Phys. Rev.* B **36** 3373
[7] MercerJ L Jr and Chou M Y 1993 *Phys. Rev.* B **47** 9366
[8] Chadi D J and Martin R M 1976 *Solid State Commun.* **19** 643
[9] Harrison W A 1986 *Phys. Rev.* **34** 2787
[10] Harrison W A 1983 *Phys. Rev.* B **27** 3592
[11] Robertson J 1983 *Phil. Mag.* B 47 33
[12] Papaconstantopoulos D A 1986 *Handbook of the Band Structure of Complex Systems (Proc. NATO Advanced Study Institute)* ed P Phariseau and W Temmerman (New York: Plenum)
[13] Sawada S 1990 *Vacuum* **1** 612
[14] Goodwin L, Skinner A J and Pettifor D G 1989 *Europhys. lett.* **9** 701
[15] Galli G, Martin R M, Car R and Parrinello M 1989 *Phys. Rev. Lett.* **62** 555
[16] Galli G, Martin R M, Car R and Parrinello M 1989 *Phys. Rev. Lett.* **63** 988
[17] Wang C Z, Ho K M and Chan C T 1993 *Phys. Rev. Lett.* **70** 611
[18] Li F and Lannin J S 1990 *Phys. Rev. Lett.* **65** 1905
[19] Raghavachari K and Binkley J S 1987 *J. Chem. Phys.* **87** 2191